LETTERS

Decreased frequency of North Atlantic polar lows associated with future climate warming

Matthias Zahn[1,2] & Hans von Storch[2,3]

Every winter, the high-latitude oceans are struck by severe storms that are considerably smaller than the weather-dominating synoptic depressions[1]. Accompanied by strong winds and heavy precipitation, these often explosively developing mesoscale cyclones—termed polar lows[1]—constitute a threat to offshore activities such as shipping or oil and gas exploitation. Yet owing to their small scale, polar lows are poorly represented in the observational and global reanalysis data[2] often used for climatological investigations of atmospheric features and cannot be assessed in coarse-resolution global simulations of possible future climates. Here we show that in a future anthropogenically warmed climate, the frequency of polar lows is projected to decline. We used a series of regional climate model simulations to downscale a set of global climate change scenarios[3] from the Intergovernmental Panel of Climate Change. In this process, we first simulated the formation of polar low systems in the North Atlantic and then counted the individual cases. A previous study[4] using NCEP/NCAR re-analysis data[5] revealed that polar low frequency from 1948 to 2005 did not systematically change. Now, in projections for the end of the twenty-first century, we found a significantly lower number of polar lows and a northward shift of their mean genesis region in response to elevated atmospheric greenhouse gas concentration. This change can be related to changes in the North Atlantic sea surface temperature and mid-troposphere temperature; the latter is found to rise faster than the former so that the resulting stability is increased, hindering the formation or intensification of polar lows. Our results provide a rare example of a climate change effect in which a type of extreme weather is likely to decrease, rather than increase.

Polar lows develop as disturbances in low-level air flows of (for example) orographic or baroclinic origin[1,6,7], which later amplify by convective processes[1,8,9] under the influence of large vertical temperature gradients. Oceanic energy loss elicited by latent and sensible heat fluxes can influence Greenland Deep Water formation and thus deep ocean circulation[10].

Typical large-scale conditions favouring polar low development are cold air outbreaks, in which cold and dry air masses originating from ice-covered regions are advected towards the open ocean. It is therefore likely that changes in large-scale parameters that favour polar low development will also influence the frequency of polar lows and can thus affect the strategy of offshore activities in the Arctic and Subarctic regions. Changes in the frequency of small-scale atmospheric systems are usually derived from large-scale proxy data, as has been done for thunderstorms in the USA[11] or for polar lows in the North Atlantic[12,13]. Studies based on simulated individual mesoscale storms are lacking so far.

An analysis of a dynamical downscaling effort, in which a regional climate model was processing NCEP/NCAR re-analysis data[5] for the period 1948–2006, found that indeed many polar lows were realistically formed[4]. This simulation, henceforth named REA, generated an average number of 56 polar lows and high inter-seasonal variability (standard deviation ±13), but no long-term trend in the number of seasonal polar low occurrences. A comparison of this model-based climatology with observed data is difficult because of the inhomogeneous and often subjective character of past weather analysis, in particular when smaller-scale features such as polar lows are concerned. However, comparison with analyses using satellite data for a
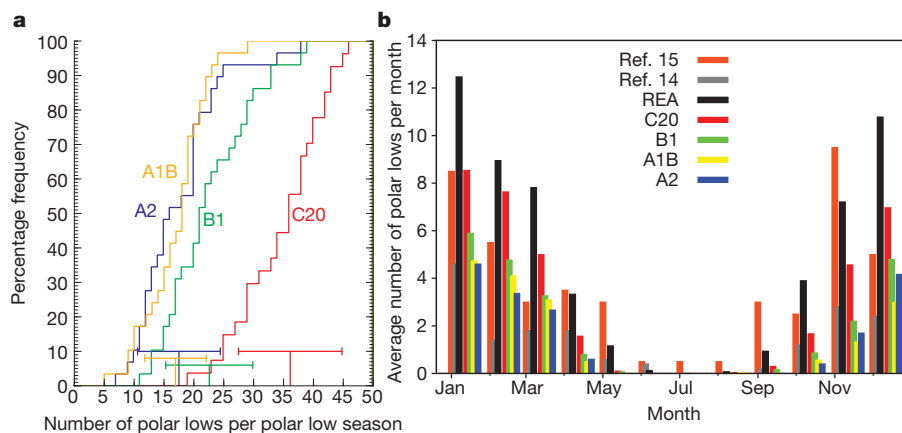
Figure 1 | Number of polar lows per polar low season and the seasonal cycle. a, Cumulative frequency of the number of polar lows resulting from the IPCC C20 scenario (red) and future scenarios B1 (green), A1B (yellow) and A2 (blue). Vertical error bars denote means and horizontal error bars denote the standard deviation. **b**, Average number of polar lows per month from observations[14,15] (orange and grey), from REA[4] (black) and from the IPCC scenarios (red, green, yellow and blue).

[1]Environmental Systems Science Centre, University of Reading, 3 Earley Gate, Reading, Berkshire RG6 6AL, UK. [2]Institute for Coastal Research/System Analysis and Modelling, GKSS-Research Centre, Max-Planck-Strasse 1, D-21502 Geesthacht, Germany. [3]Meteorological Institute, University of Hamburg, Bundesstrasse 55, D-20146 Hamburg, Germany.
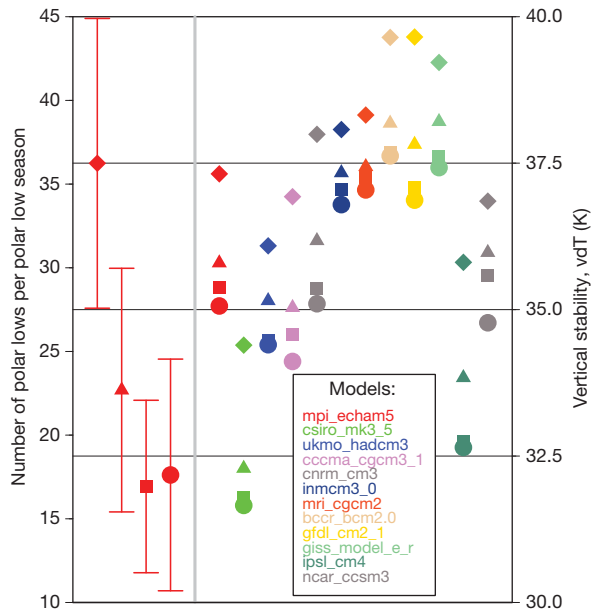
Figure 2 | Projected changes in polar low frequency and vertical atmospheric stability. The left panel shows the average number and standard deviation of polar lows per polar low season. The right panel shows the mean static/vertical stability as given by the vertical temperature difference (vdT) between sea surface and air at 500 hPa (in Kelvin) for the period October to March over 30 years (1960–1989 for IPCC-AR4 scenario C20 and 2070–2099 for scenarios B1, A1B and A2). Vertical stability is calculated over ice-free ocean grid cells in our simulation area. Data are derived from four IPCC scenarios: C20 (diamonds), B1 (triangles), A1B (squares) and A2 (circles).

few years[14,15] (1978–1982, 2004–2005) returned encouraging qualitative similarities (Supplementary Fig. 2). Also, the spatial pattern with three density maxima, one between Greenland and Iceland, one south of Iceland and a third off the Norwegian coast, is consistent with previous studies[16]. We conclude that the approach of dynamically

downscaling large-scale information with a regional climate model is skilful in generating realistic statistics of polar lows.

For the assessment of polar low frequency for different scenarios of a warmed climate, we downscaled two periods of transient simulations conducted for the Fourth Assessment Report (AR4) of the Intergovernmental Panel of Climate Change (IPCC) with the ECHAM5/MPI-OM model[17,18]. First, a 30-year control period driven by greenhouse gas concentrations valid for 1960–1989 was downscaled and serves as a reference (C20). Second, another 30-year period, this time driven by three of the most commonly used IPCC-AR4 greenhouse-gas future concentration scenarios[3]—B1, A1B and A2—was downscaled as well. Again, polar lows formed in all of these regional climate simulations (Fig. 1).

The average number of polar lows in C20 is only approximately 36 polar lows per polar low season (PLS) (see Methods and left-hand side of Fig. 2), which is considerably fewer than that found in the REA simulation. This systematic difference is related to the difference in mean vertical stability, which is also considerably biased in C20 compared to REA (Supplementary Fig. 4). It is evident that more polar lows in REA coincide with lower mean vertical stability. This situation is reversed in C20, where fewer polar lows coincide with higher vertical stability.

Biases between different IPCC future climate model simulations, and also between present climate simulations and reanalysis or observations are common and are referred to in the IPCC-AR4 report[19,20] or have been investigated[21]. These biases can result from different physics and parametrizations involved in the different formulation of the models. To overcome this issue, here we use the delta method, which compares time slices of simulated IPCC future scenarios relative to a simulated IPPC twentieth-century scenario of the same model. Thus, the physics and parametrizations remain consistent in our experiment. Despite these biases, the REA and the IPCC simulations show a similar annual cycle of polar low formation, with the large majority forming in the cold season (Fig. 1b). Further joint statistical properties of REA and C20 include large interannual variability, the absence of any significant trend and spatial patterns with their three main centres of action (Fig. 3a).
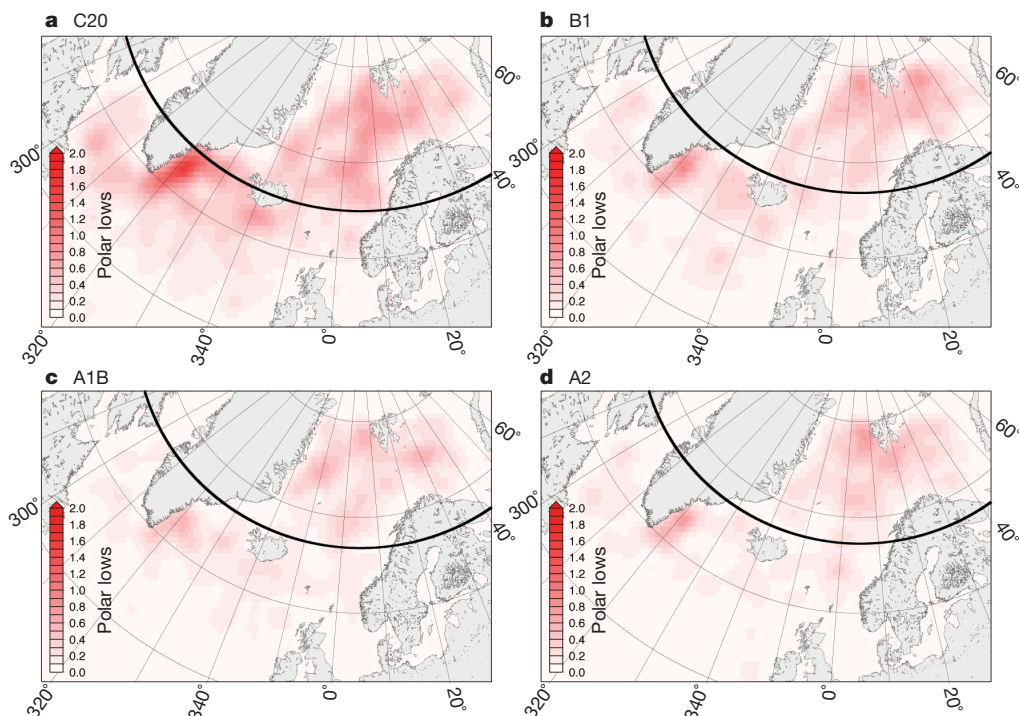
Figure 3 | Polar low density distribution. IPCC scenarios: **a**, C20; **b**, B1; **c**, A1B; **d**, A2. The colour scale measures detected polar lows per 2,500 km². The thick black line in each panel indicates the mean latitude of polar low genesis.

Table 1 | Mean latitude and standard deviation of ice edge and polar low genesis.

IPCC scenario	Mean latitude of ice edge (°N)	Standard deviation, s.d.	Mean latitude of polar low genesis* (°N)	s.d.	Mean latitude of polar low genesis over the whole North Atlantic** (°N)	s.d.
C20	75.36	±0.69	68.49	±6.17	64.94	±7.42
B1	77.99	±0.69	69.84	±6.48	66.84	±8.07
A1B	79.82	±0.64	70.28	±6.55	66.81	±8.50
A2	79.27	±0.90	70.63	±6.70	67.27	±8.54

The ice edge is given by the −1.7 °C isotherm of the mean sea surface temperature per polar low season and is calculated for the North Atlantic between 20° W and 20° E. The mean latitude of polar low genesis is given between these longitudes (20° W and 20° E) only (*) as well as for the whole simulation area covering the whole North Atlantic (see Supplementary Fig.1) (**). The mean latitude of ice edge and polar low genesis are significantly different at the 99.5% level in all the downscaled IPCC projections compared to C20.

Because of the consistent biases in the global model, we derive our estimate of future change in polar low frequency by comparing three downscaled IPCC scenarios (B1, A1B and A2) with the control simulation C20 as a reference. Because the data of these scenarios were all delivered by the ECHAM5/MPI-OM-model, the driving data share the same physics and parametrization and thus remain consistent over time. All of the future scenarios experience a reduction of the number of polar lows per PLS during 2070–2099, resulting in average numbers of 22.7, 16.9 and 17.6 in scenarios B1, A1B and A2, respectively (left-hand side of Fig. 2). According to a *t*-test based on their seasonal distributions (Fig. 1), all of these average numbers are statistically significantly different (at the 99.5% level) from the mean in C20. The greenhouse-gas concentrations and atmospheric warming curves in A1B and A2 are similar, or even slightly higher in A1B than in A2, until about 2070. At that time, the two curves diverge, because A1B assumes a decrease in world population and greenhouse-gas emissions and thus slower rising concentrations from the middle of the twenty-first century onwards. The resulting more slowly rising temperatures affect polar low frequency in the last 15 years (PLS 2085–2099). Here, slightly lower average numbers of polar lows per PLS form in A2 (15.5 cases) compared to A1B (16.3 cases).

The warming climate not only significantly affects the number of polar lows per PLS, but also changes their spatial distribution (Fig. 3). The density maximum south of Iceland disappears in all of the future scenarios and the maximum between Iceland and Greenland loses its dominance compared to the maximum in the Norwegian Sea. Further, the density centre in the Barents Sea southeast of Spitsbergen shifts farther north into the Greenland Sea, west of Spitsbergen, in the future scenarios. The projected northward shift of polar low activity may be quantified by the mean latitude of polar low genesis—which is 64.9 °N in C20 and 66.8 °N, 66.8 °N and 67.3 °N in scenarios B1, A1B and A2 (Table 1), respectively. This shift is about 2° northward and is statistically different at the 99.5% level for all these cases.

To understand the dynamical reason for this weakening and northward shift of polar low activity in projected future climate compared to C20, we have examined the changes of the temperature at the ocean surface (SST) and in the troposphere, as represented by conditions at about 500 hPa. In contrast to the globally warming oceans, parts of the North Atlantic, such as between Iceland and Greenland, have been cooling during recent decades[22–24]. According to the IPCC-AR4 scenarios[19], the North Atlantic is expected to experience a comparatively moderate warming, whereas tropospheric air temperature is expected to warm more quickly than the global average air temperature in the Arctic[19]. This tendency of a more slowly warming ocean leads to increased vertical stability, which is less favourable for the formation of polar lows. As an indicator for this stability, we calculated the temperature differences of the area and time-averaged ice-free SST and 500-hPa air temperature over the maritime northern North Atlantic of our simulation area during the main polar low months, October to March (right-hand side of Fig. 2). Here a lower difference means higher stability. It is evident that mean vertical stability is projected to rise with increasing greenhouse-gas concentration and climate warming. This holds for the scenarios of the ECHAM5/MPI-OM driving model as well as for all further model data of the IPCC-AR4 provided by the World Climate Research Program's Coupled Model Intercomparison Project phase 3 (WCRP

CMIP3) multi-model data set. The results also hold for subregions around the density maxima south of Spitsbergen and between Iceland and Greenland (Supplementary Information and Supplementary Fig. 3).

Under present conditions, shallow baroclinic zones along the Arctic ice edge frequently provide initial conditions for polar lows in the northern North Atlantic[1,25]. Consistent with the projected northward shift of the Arctic ice edge (Table 1), a projected northward shift of cold air outbreaks[12] and of North Atlantic storms in general[26], the area of polar low formation has also shifted northward in the investigated IPCC-AR4 futures.

METHODS SUMMARY

To properly resolve and count polar lows, data from IPCC future emission scenarios as given by the IPCC-AR4 ECHAM5/MPI-OM[17,18] experiments were dynamically scaled down with the regional climate model CLM[27] to a grid cell size of about 50×50 km^2. The scenarios applied over the 2070–2099 period are B1, A1B and A2, as described in the IPCC Special Report on Emission Scenarios[3]. These are compared to the corresponding 1960–1989 greenhouse-gas scenario, also run by the IPCC-AR4 ECHAM5/MPI-OM experiments. The results of this control experiment are compared to a polar low database originating from a former work[4] with a similar approach but using NCEP/NCAR re-analysis data[5]. To identify polar lows, a detection algorithm based on the positions of the minima in digitally bandpass-filtered[28] mean sea level pressure output fields of the CLM was applied[29,30]. Northern Hemisphere polar lows are phenomena of the cold season. In none of the simulations was any polar low found in the summer months of June and July (Fig. 1b). To avoid splitting into two years the polar lows occurring in a given winter, we aggregate the polar low frequencies of each winter and invent the term PLS, here denoting the period from July to June of the following year. A given PLS is assigned to the second year. We note that this procedure results in 29 PLSs, because the first and last six months of the simulation period are dismissed from the analysis. For further details, see Supplementary Information.

1. Rasmussen, E. A. & Turner, J. *Polar Lows: Mesoscale Weather Systems in the Polar Regions* (Cambridge Univ. Press, 2003).
2. Condron, A., Bigg, G. R. & Renfrew, I. A. Polar mesoscale cyclones in the northeast Atlantic: comparing climatologies from ERA-40 and satellite imagery. *Mon. Weath. Rev.* **134**, 1518–1533 (2006).
3. Nakicenovic, N. & Swart, R. *IPCC Special Report on Emissions Scenarios* (Cambridge Univ. Press, 2000).
4. Zahn, M. & von Storch, H. A long-term climatology of North Atlantic polar lows. *Geophys. Res. Lett.* **35**, L22702 (2008).
5. Kalnay, E. *et al.* The NCEP/NCAR 40-year reanalysis project. *Bull. Am. Meteorol. Soc.* **77**, 437–471 (1996).
6. Harrold, T. W. & Browning, K. A. The polar low as a baroclinic disturbance. *Q. J. R. Meteorol. Soc.* **95**, 710–723 (1969).
7. Klein, T. & Heinemann, G. Interaction of katabatic winds and mesocyclones near the eastern coast of Greenland. *Meteorol. Appl.* **9**, 407–422 (2002).
8. Emanuel, K. A. & Rotunno, R. Polar lows as arctic hurricanes. *Tellus A* **41**, 1–17 (1989).
9. Rasmussen, E. A. The polar low as an extratropical CISK disturbance. *Q. J. R. Meteorol. Soc.* **105**, 531–549 (1979).
10. Condron, A., Bigg, G. R. & Renfrew, I. A. Modeling the impact of polar mesocyclones on ocean circulation. *J. Geophys. Res.* **113**, doi: 10.1029/2007JC004599 (2008).
11. Trapp, R. J. *et al.* Changes in severe thunderstorm environment frequency during the 21st century caused by anthropogenically enhanced global radiative forcing. *Proc. Natl Acad. Sci. USA* **104**, 19719–19723 (2007).
12. Kolstad, E. W. & Bracegirdle, T. J. Marine cold-air outbreaks in the future: an assessment of IPCC AR4 model results for the Northern Hemisphere. *Clim. Dyn.* **30**, 871–885 (2008).

13. Vavrus, S., Walsh, J. E., Chapman, W. L. & Portis, D. The behavior of extreme cold air outbreaks under greenhouse warming. *Int. J. Climatol.* **26,** 1133–1147 (2006).

14. Wilhelmsen, K. Climatological study of gale-producing polar lows near Norway. *Tellus A* **37,** 451–459 (1985).

15. Blechschmidt, A.-M. A 2-year climatology of polar low events over the Nordic seas from satellite remote sensing. *Geophys. Res. Lett.* **35,** L09815 (2008).

16. Bracegirdle, T. & Gray, S. An objective climatology of the dynamical forcing of polar lows in the Nordic seas. *Int. J. Climatol.* **28,** 1903–1919 (2008).

17. Roeckner, E. *et al.* The atmospheric general circulation model ECHAM 5. Part I: Model description. MPI report 349 〈http://www.mpimet.mpg.de/fileadmin/ models/echam/mpi_report_349.pdf〉 (Max-Planck Institute, 2003).

18. Marsland, S. J., Haak, H., Jungclaus, J. H., Latif, M. & Röske, F. The Max-Planck-Institute global ocean/sea ice model with orthogonal curvilinear coordinates. *Ocean Model.* **5,** 91–127 (2003).

19. Meehl, G. A. *et al.* in *Climate Change 2007: The Physical Science Basis* (eds Solomon, S. *et al.*) 747–845 (Cambridge Univ. Press, 2007).

20. Christensen, J. H. *et al.* in *Climate Change 2007: The Physical Science Basis* (eds Solomon, S. *et al.*) 847–940 (Cambridge Univ. Press, 2007).

21. Jun, M., Knutti, R. & Nychka, D. W. Spatial analysis to quantify numerical model bias and dependence. *J. Am. Stat. Assoc.* **103,** 934–947 (2008).

22. Levitus, S., Antonov, J., Boyer, T. P. & Stephens, C. Warming of the world ocean. *Science* **287,** 2225–2229 (2000).

23. Levitus, S., Antonov, J. & Boyer, T. Warming of the world ocean, 1955– 2003. *Geophys. Res. Lett.* **32,** L02604 (2005).

24. Bindoff, N. L. *et al.* in *Climate Change 2007: The Physical Science Basis* (eds Solomon, S. *et al.*) 385–428 (Cambridge Univ. Press, 2007).

25. Heinemann, G. On the development of wintertime meso-scale cyclones near the sea ice front in the Arctic and Antarctic. *Glob. Atmos.-Ocean Syst.* **4,** 89–123 (1996).

26. Bengtsson, L., Hodges, K. I. & Roeckner, E. Storm tracks and climate change. *J. Clim.* **19,** 3518–3543 (2006).

27. Rockel, B., Will, A. & Hense, A. The regional climate model COSMO-CLM (CCLM). *Meteorol. Z.* **17,** 347–348 (2008).

28. Feser, F. & von Storch, H. A spatial two-dimensional discrete filter for limited-area-model evaluation purposes. *Mon. Weath. Rev.* **133,** 1774–1786 (2005).

29. Zahn, M. & von Storch, H. Tracking polar lows in CLM. *Meteorol. Z.* **17,** 445–453 (2008).

30. Zahn, M., von Storch, H. & Bakan, S. Climate mode simulation of North Atlantic polar lows in a limited area model. *Tellus A* **60,** 620–631 (2008).

Author Contributions Both authors contributed to developing the ideas presented. M.Z. did the technical work for this study.

Author Information Reprints and permissions information is available at www.nature.com/reprints. The authors declare no competing financial interests. Readers are welcome to comment on the online version of this article at www.nature.com/nature. Correspondence and requests for materials should be addressed to M.Z. (matthias.zahn@gkss.de).